Weierstraß-Institut
für Angewandte Analysis und Stochastik

im Forschungsverbund Berlin e.V.

Preprint ISSN 0946 – 8633

Efficient treatment of stationary free boundary problems

Karsten Eppler[1] and Helmut Harbrecht[2]

submitted: 20th September 2004

[1] Weierstraß-Institut für Angewandte Analysis und Stochastik
Mohrenstr. 39
10117 Berlin
Germany
E-Mail: eppler@wias-berlin.de

[2] Institut für Informatik
und Praktische Mathematik
Christian–Albrechts–Universität zu Kiel
Olshausenstr. 40
24098 Kiel
Germany
E-Mail: hh@numerik.uni-kiel.de

No. 965
Berlin 2004

2000 *Mathematics Subject Classification.* 49Q10, 49M15, 65N38, 49K20.

Key words and phrases. free boundary problem, shape calculus, Newton method, boundary integral equations, multiscale methods, sufficient second order conditions.

This research has been carried out when the second author stayed at the Department of Mathematics, University Utrecht, Netherlands, supportet by the EU-IHP project *Nonlinear Approximation and Adaptivity: Breaking Complexity in Numerical Modelling and Data Representation.*

Edited by
Weierstraß-Institut für Angewandte Analysis und Stochastik (WIAS)
Mohrenstraße 39
10117 Berlin
Germany

Fax: + 49 30 2044975
E-Mail: preprint@wias-berlin.de
World Wide Web: http://www.wias-berlin.de/

ABSTRACT. In the present paper we consider the efficient treatment of free boundary problems by shape optimization. We reformulate the free boundary problem as shape optimization problem. A second order shape calculus enables us to realize a Newton scheme to solve this problem. In particular, all evaluations of the underlying state function are required only on the boundary of the domain. We compute these data by boundary integral equations which are numerically solved by a fast wavelet Galerkin scheme. Numerical results prove that we succeeded in finding a fast and robust algorithm for solving the considered class of problems. Furthermore, the stability of the solutions is investigated by treating the second order sufficient optimality conditions of the underlying shape problem.

1. INTRODUCTION

Let $T \subset \mathbb{R}^n$ denote a bounded domain with boundary $\partial T = \Gamma$. Inside the domain T we assume the existence of a simply connected subdomain $S \subset T$ with boundary $\partial S = \Sigma$. The resulting annular domain $T \setminus \overline{S}$ is denoted by Ω. The topological situation is visualized in Figure 1.1.

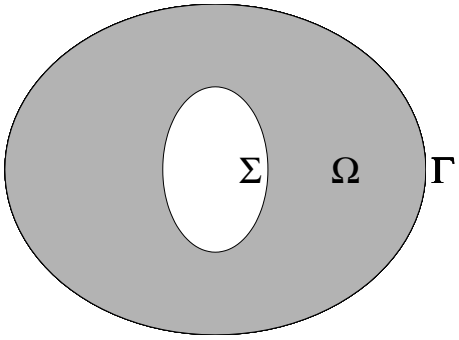

FIGURE 1.1. The domain Ω and its boundaries Γ and Σ.

We consider the following overdetermined boundary value problem in the annular domain Ω

$$\begin{aligned} -\Delta u &= f && \text{in } \Omega, \\ \|\nabla u\| &= g && \text{on } \Gamma, \\ u &= 0 && \text{on } \Gamma, \\ u &= h && \text{on } \Sigma, \end{aligned} \tag{1.1}$$

where $g, h > 0$ and $f \geq 0$ are sufficiently smooth functions such that $u \in C^(\overline{\Omega})$. We like to stress that the Dirichlet data imply that u is positive in Ω and negative in $\mathbb{R}^n \setminus T$. Hence, there holds the identity

$$\|\nabla u\| \equiv -\frac{\partial u}{\partial \mathbf{n}} \qquad \text{on } \Gamma$$

since u admits homogeneous Dirichlet data on Γ.

We arrive at a free boundary problem if the boundary Γ is the unknown. In other words, we seek a domain Ω with fixed boundary Σ and unknown boundary Γ such that the overdetermined boundary value problem (1.1) is solvable. For the existence of solutions we refer the reader to e.g. [1, 24].

Shape optimization provides an efficient tool to solve such free boundary value problems, cf. [14, 28, 38, 39]. Considering the cost functional

$$J(\Omega) = \int_\Omega \|\nabla u\|^2 + g^2 d\mathbf{x} \tag{1.2}$$

with underlying *state equation*

$$\begin{aligned} -\Delta u &= f \qquad \text{in } \Omega, \\ u &= 0 \qquad \text{on } \Gamma, \\ u &= h \qquad \text{on } \Sigma, \end{aligned} \tag{1.3}$$

the solution of the free boundary problem is equivalent to the shape optimization problem

$$J(\Omega) \to \min. \tag{1.4}$$

This issues from the necessary condition of a minimizer of the cost functional (1.2), that is,

$$\nabla J(\Omega)[\mathbf{V}] = \int_\Gamma \langle \mathbf{V}, \mathbf{n} \rangle \left\{ g^2 - \left[\frac{\partial u}{\partial \mathbf{n}} \right]^2 \right\} d\sigma = 0 \tag{1.5}$$

has to be valid for all sufficiently smooth perturbation fields $\mathbf{V}$. Hence, via shape optimization a variational formulation of the condition

$$\frac{\partial u}{\partial \mathbf{n}} = -g \qquad \text{on } \Gamma \tag{1.6}$$

is induced. However, it is well known that a stationary domain $\Omega^\star$ of the minimization problem (1.2), (1.3) is a stable minimum if and only if the shape Hessian is $H^{1/2}(\Gamma^\star)$-coercive at this domain, see [13].

The problem under consideration can be viewed as the prototype of a free boundary problem arising in many applications where we introduced the fixed boundary Σ only to ensure uniqueness of the solution. The growth of anodes in electrochemical processes might be modeled like above with $f \equiv 0$ and $g, h \equiv 1$. In the two dimensional exterior magnetic shaping of liquid metals the state equation is an exterior boundary value problem and the uniqueness is ensured by a volume constraint of the domain Ω [7, 20, 32, 33]. The maximization of the torsional stiffness of a elastic cylindrical bar under simultaneous constraints on its volume and bending rigidity fits also in the above general setup, see [2, 18, 19] for the details. The detection of voids or inclusions in 2d or 3d electrical impedance tomography is slightly different since the roles of Σ and Γ are interchanged [22, 23, 34]. Moreover, this inverse problem is severely ill-posed, in contrary to the present class of problems. We refer the reader to [3, 4, 5, 29] and the references therein for further details. We emphasize that electromagnetic shaping and other important applications in three dimensions are not included in our setup since the state equation (1.3) is in

general a Neumann problem. Therefore, and also for sake of simplicity, we will restrict ourselves in the present paper to two spatial dimensions. The application to the higher dimensional case is straightforward, see also Remark 5.2. We like to stress that the present method applies not only to the Laplacian, but also to differential operators with known fundamental solution, like the Stokes, Helmholtz or Lamé operator.

Computing the shape Hessian of the cost functional (1.2) enables us to perform a Newton scheme to solve the shape problem (1.4). In fact, as shown in [19], a Newton scheme is much more accurate and efficient in comparison to first order optimization methods since a line-search becomes nearly obsolete. However, the state equation has to be solve very often on different domain during the iteration process. Nevertheless, we will show that all quantities, the cost functional as well as its gradient and Hessian require only boundary data of the state function. Hence, introducing a suitable Newton potential to resolve the inhomogenity, the state equation (1.3) can be solved efficiently by a boundary element method. We apply a *wavelet Galerkin scheme* which produces approximate solutions within discretization error accuracy offered by the underlying Galerkin method at a computational expense that stays proportional to the number of unknowns, [11, 25, 27, 35]. As it is shown in [19, 20], this results in powerful second order shape optimization algorithms.

The paper is organized as follows. Section 2 is dedicated to the second order shape calculus. In Section 3 we derive sufficient conditions to verify stable minimizers. Then, we overview in Section 4 how to derive first and second order derivatives of the state function by boundary integral equations. In Section 5 we introduce the discretization of the boundary and the wavelet Galerkin scheme. In Section 6, we present numerical results. Finally, in Section 7 we state concluding remarks.

2. Shape Calculus

First we introduce some notation. For a given domain $D \in \mathbb{R}^n$ the space $C^2(\overline{D})$ consists of all two times continuously differentiable functions $f : \overline{D} \to \mathbb{R}^m$. A function $f \in C^2(\overline{D})$ belongs to $C^{2,\alpha}(\overline{D})$, if the (spatial) Hessian $\nabla^2 f$ is Hölder continuous with coefficient $0 < \alpha \leq 1$. A domain $D \in \mathbb{R}^2$ is of class $C^{2,\alpha}$ if for each $x \in \partial D$ a neighbourhood $U(x) \subseteq \partial\Omega$ and a diffeomorphism $\gamma : [0,1] \to \overline{U(x)}$ exists such that $\gamma \in C^{2,\alpha}([0,1])$, see [41] for example.

Next, we adopt the shape calculus developed in [15, 16] to our model problem, see also [14, 38] and the references therein for a general background on shape optimization. It suffices to consider $S \in C^{0,1}$ but due to a second order boundary perturbation calculus, we have to assume $T \in C^{2,\alpha}$ for some fixed $\alpha \in (0,1)$ in contrast to $T \in C^2$ for the first order calculus. Clearly, since the boundary Σ is fixed, the domain Ω can be identified with a function which describes the free boundary Γ. For sake of simplicity, we assume that the domain T is starlike with respect to $\mathbf{0}$. Then, we can parametrize Γ via polar coordinates

$$\Gamma := \left\{ \boldsymbol{\gamma}(\phi) = r(\phi) \left[\begin{smallmatrix} \cos\phi \\ \sin\phi \end{smallmatrix} \right] : \phi \in [0, 2\pi] \right\},$$

where $r \in C^{2,\alpha}_{\rm per}[0,2\pi]$ is a positive function such that $\mathrm{dist}(\Sigma,\Gamma) > 0$ and $C^{2,\alpha}_{\rm per}[0,2\pi] = \{r \in C^{2,\alpha}[0,2\pi] : r^{(i)}(0) = r^{(i)}(2\pi),\ i = 0,1,2\}$. The tangent and normal to Γ are computed by

$$\mathbf{t} = \frac{r'\left[\begin{smallmatrix}\cos\phi\\ \sin\phi\end{smallmatrix}\right] + r\left[\begin{smallmatrix}-\sin\phi\\ \cos\phi\end{smallmatrix}\right]}{\sqrt{r^2+r'^2}}, \qquad \mathbf{n} = \frac{r'\left[\begin{smallmatrix}\sin\phi\\ -\cos\phi\end{smallmatrix}\right] + r\left[\begin{smallmatrix}\cos\phi\\ \sin\phi\end{smallmatrix}\right]}{\sqrt{r^2+r'^2}}.$$

We consider $dr \in C^{2,\alpha}_{\rm per}[0,2\pi]$ as standard variation for perturbed domains Ω_ε and boundaries Γ_ε, respectively, defined by $r_\varepsilon(\phi) = r(\phi) + \varepsilon dr(\phi)$, where $\boldsymbol{\gamma}_\varepsilon(\phi) = r_\varepsilon(\phi)\mathbf{e}_r(\phi)$ is always a Jordan curve. Herein, $\mathbf{e}_r(\phi) = [\cos\phi, \sin\phi]^T$ denotes the unit vector in the outer radial direction. The main advantage of this simple approach is a complete embedding of the shape problem into a Banach space setting. That is, *both* the shapes and its increments, can be viewed as elements of $C^{2,\alpha}_{\rm per}[0,2\pi]$.

The shape gradient of the cost functional in (1.2) becomes in polar coordinates

$$\nabla J(\Omega)[dr] = \int_0^{2\pi} dr\, r \left\{ g^2 - \left[\frac{\partial u}{\partial \mathbf{n}}\right]^2 \right\} d\phi. \tag{2.7}$$

It is a functional in $H^{-1/2}(\Gamma)$ living only on the free boundary Γ. The shape Hessian is a continuous bilinear form on $H^{1/2}(\Gamma) \times H^{1/2}(\Gamma)\times$, namely

$$\begin{aligned}\nabla^2 J(\Omega)[dr_1, dr_2] = \int_0^{2\pi} dr_1 dr_2 \Bigg\{ & g^2 - \left[\frac{\partial u}{\partial \mathbf{n}}\right]^2 + 2rg\langle \nabla g, \mathbf{e}_r\rangle \\ & - \frac{2r}{\sqrt{r^2+r'^2}} \frac{\partial u}{\partial \mathbf{n}} \left[r \frac{\partial^2 u}{\partial \mathbf{n}^2} + r' \frac{\partial^2 u}{\partial \mathbf{n}\partial \mathbf{t}} \right] \Bigg\} - 2r\, dr_1 \frac{\partial u}{\partial \mathbf{n}} \cdot \frac{\partial du[dr_2]}{\partial \mathbf{n}} d\phi.\end{aligned} \tag{2.8}$$

Herein, the *local shape derivative* $du = du[dr_2]$ of the state function satisfies

$$\begin{aligned} \Delta du &= 0 && \text{in } \Omega, \\ du &= 0 && \text{on } \Sigma, \\ du &= -dr_2\, \langle \mathbf{e}_r, \mathbf{n}\rangle \tfrac{\partial u}{\partial \mathbf{n}} && \text{on } \Gamma. \end{aligned} \tag{2.9}$$

Notice that $\partial^2 u/\partial \mathbf{n}^2 := \langle \nabla^2 u \cdot \mathbf{n}, \mathbf{n}\rangle$ and $\partial^2 u/(\partial \mathbf{n}\partial \mathbf{t}) := \langle \nabla^2 u \cdot \mathbf{n}, \mathbf{t}\rangle$.

3. Stability of Minimizers

Let $\Omega^\star$, associated with the radial function $r^\star$, be a stationary domain, i.e., the necessary condition

$$\nabla J(\Omega^\star)[dr] \equiv 0 \tag{3.10}$$

holds for all directions dr. Then, there holds the following Taylor expansion for all domains Ω, described by $r = r^\star + dr$, in a neighbourhood of a stationary domain $\Omega^\star$

$$J(\Omega) - J(\Omega^\star) = 0 + \nabla^2 J(\Omega^\star)[dr, dr]/2 + \eta. \tag{3.11}$$

Herein, the second order Taylor remainder (cf. [13]) satisfies

$$2|\eta| = \left|\nabla^2 J(\Omega_t)[dr, dr] - \nabla^2 J(\Omega^\star)[dr, dr]\right| \le \omega(\|dr\|_{C^{2,\alpha}}) \|dr\|^2_{H^{1/2}([0,2\pi])}, \tag{3.12}$$

where Ω_t is given via $r_t = r^\star + t dr$, $t \in (0,1)$, and $\omega(t) \to 0$ if $t \to 0$.

The following lemma is concerned with the sufficient optimality condition, cf. [13].

Lemma 3.1. *The stationary domain $\Omega^\star$ is a local minimum, if the shape Hessian is $H^{1/2}(\Gamma^\star)$-coercive, that is*

$$\nabla^2 J(\Omega^\star)[dr, dr] \geq c\|dr\|^2_{H^{1/2}([0,2\pi])} \tag{3.13}$$

for some constant $c > 0$.

We emphasize that the radial function $r^\star$ has to be in $C^{2,\alpha}_{\mathrm{per}}([0, 2\pi])$ to ensure the estimate (3.11) and (3.12), while a minimizer is stable if the shape Hessian is $H^{1/2}(\Gamma^\star)$-coercive. For further considerations of this lack of regularity in shape optimization, called *two-norm discrepancy*, we refer to [13, 17].

To investigate the coercivity condition (3.13) for the problem under consideration, we simplify first the shape Hessian at the stationary domain.

Lemma 3.2. *We introduce the multiplication operator*

$$Mdr := dr \cdot \frac{gr^\star}{\sqrt{r^{\star 2} + r^{\star\prime 2}}} \tag{3.14}$$

and the Dirichlet-to-Neumann map

$$\Lambda(Mdr) := \frac{\partial du[dr]}{\partial \mathbf{n}}\Big|_{\Gamma^\star} \tag{3.15}$$

with respect to the Dirichlet data Mdr and 0 on $\Gamma^\star$ and Σ, respectively. With these operators at hand, the Hessian at the stationary domain $\Omega^\star$ admits the representation

$$\nabla^2 J(\Omega^\star)[dr_1, dr_2] = \int_{\Gamma^\star} (Mdr_1) \left\{ \Lambda + \kappa + \left[\frac{\partial g}{\partial \mathbf{n}} - f\right] \Big/ g \right\} (Mdr_2) d\phi, \tag{3.16}$$

where κ denotes the curvature of $\Gamma^\star$.

Proof. From $\partial u/\partial \mathbf{n} = -g$ we conclude

$$\begin{aligned}\nabla^2 J(\Omega^\star)[dr_1, dr_2] &= 2\int_0^{2\pi} r^\star\, dr_1 g \cdot \frac{\partial du[dr_2]}{\partial \mathbf{n}} \\ &\quad + r^\star dr_1 dr_2 g \left\{ \langle \nabla g, \mathbf{e}_{r^\star}\rangle + \frac{1}{\sqrt{r^{\star 2} + r^{\star\prime 2}}} \left[r^\star \frac{\partial^2 u}{\partial \mathbf{n}^2} + r^{\star\prime} \frac{\partial^2 u}{\partial \mathbf{n}\partial \mathbf{t}} \right] \right\} d\phi.\end{aligned}$$

We denote differentiation with respect to the arclength by $\partial/\partial s$. Then, the homogeneous Dirichlet data of u at Γ imply

$$-\frac{\partial g}{\partial \mathbf{t}} = -\frac{\partial g}{\partial s} = \frac{\partial}{\partial s}\left(\frac{\partial u}{\partial \mathbf{n}}\right) = \kappa \frac{\partial u}{\partial \mathbf{t}} + \frac{\partial^2 u}{\partial \mathbf{n}\partial \mathbf{t}} = \frac{\partial^2 u}{\partial \mathbf{n}\partial \mathbf{t}}.$$

Combining this result with

$$\langle \nabla g, \mathbf{e}_{r^\star}\rangle = \left[r^\star \frac{\partial g}{\partial \mathbf{n}} + r^{\star\prime} \frac{\partial g}{\partial \mathbf{t}} \right] \Big/ \sqrt{r^{\star 2} + r^{\star\prime 2}}$$

we deduce

$$\langle \nabla g, \mathbf{e}_{r^\star} \rangle + \frac{r^{\star\prime}}{\sqrt{r^{\star 2} + r^{\star\prime 2}}} \frac{\partial^2 u}{\partial \mathbf{n} \partial \mathbf{t}} = \frac{r^\star}{\sqrt{r^{\star 2} + r^{\star\prime 2}}} \frac{\partial g}{\partial \mathbf{n}}$$

Next, due to homogeneous boundary conditions at $\Gamma^\star$, we find

$$\frac{\partial^2 u}{\partial \mathbf{n}^2} = -\kappa \frac{\partial u}{\partial \mathbf{n}} - f = \kappa g - f,$$

see [19] for the details. Observing that the surface measure is given by $\sqrt{r^{\star 2} + r^{\star\prime 2}}$, we get the final result. □ □

Lemma 3.3. *The multiplication operator M defined in* (3.14) *is a continuous and bijective mapping from $H^{1/2}(\Gamma)$ to $H^{1/2}(\Gamma)$.*

Proof. Abbreviating $u := gr^\star / \sqrt{r^{\star 2} + r^{\star\prime 2}}$ we may write $Mdr = dr \cdot u$. Due to results of Triebel [40] or Mazja and Shaposhnikova [31], the multiplication operator M is continuous from $H^{1/2}(\Gamma)$ to $H^{1/2}(\Gamma)$ provided that $g \in C^{0,\alpha}(\Gamma)$ for some $\alpha > 1/2$. In particular, u is strictly positive which implies the bijectivity. □ □

Lemma 3.4. *The Dirichlet-to-Neumann map* (3.15) *is $H^{1/2}(\Gamma^\star)$-coercive.*

Proof. Combining the well known result (see e.g. [41])

$$\int_{\Gamma^\star} Mdr \Lambda(Mdr) d\sigma = \int_{\Omega^\star} \|\nabla du[dr]\|^2 d\mathbf{x} \geq c \|du[dr]\|^2_{H^1(\Omega^\star)/\mathbb{R}}$$

with the fact that we have homogeneous Dirichlet-data on Σ, we arrive at

$$\|du[dr]\|_{H^1(\Omega^\star)/\mathbb{R}} \sim \|Mdr\|_{H^{1/2}(\Gamma^\star)} \sim \|dr\|_{H^{1/2}(\Gamma^\star)}.$$

□ □

As an immediate consequence of these considerations, we are able to formulate the following corollary concerning the $H^{1/2}(\Gamma^\star)$-coercivity.

Corollary 3.5. *The Hessian is $H^{1/2}(\Gamma^\star)$-coercive if*

$$\kappa + \left[\frac{\partial g}{\partial \mathbf{n}} - f \right] \Big/ g \geq 0 \qquad \text{on } \Gamma, \tag{3.17}$$

In particular, in the case $g \equiv const.$ and $f \equiv 0$, the shape Hessian is $H^{1/2}(\Gamma^\star)$-coercive if the boundary $\Gamma^\star$ is convex (seen from inside).

Remark 3.6. *One the one hand, the present corollary gives only a sufficient criterion to check if a stationary domain provides a stable minimum. However,* (3.17) *denotes a criterion which can be* verified *numerically. On the other hand, we see that a nontrivial inhomogenity f with $f|_{\Gamma^\star} \not\equiv 0$ implies more instability. Let us further remark, in the case $g \equiv const.$, the derived formula is completely analogous to the results of Dambrine* [13] *in case of a volume constraint instead of prescribed Neumann data.*

At first glance the evaluation of the cost functional (1.2) seems to require the explicit knowledge of the state function u on the complete domain Ω. But in this section we show that thanks to a suitable a Newton potential the functional as well as its gradient and Hessian can be derived from the boundary data of a harmonic function.

Employing a Newton potential N_f satisfying

$$-\Delta N_f = f \qquad \text{in } \Omega, \tag{4.18}$$

the ansatz

$$u = N_f + v \tag{4.19}$$

reduces the state equation (1.3) to a Dirichlet problem for the Laplacian

$$\begin{aligned} \Delta v &= 0 && \text{in } \Omega, \\ v &= -N_f && \text{on } \Gamma, \\ v &= h - N_f && \text{on } \Sigma. \end{aligned} \tag{4.20}$$

First, we consider the cost functional. Integration by parts yields

$$J(\Omega) = \int_\Omega \|\nabla u\|^2 + g^2 d\mathbf{x} = \int_\Omega g^2 + (N_f + v) f d\mathbf{x} + \int_\Sigma \frac{\partial (N_f + v)}{\partial \mathbf{n}} h d\sigma. \tag{4.21}$$

Green's second formula implies the identity

$$\int_\Omega v f d\mathbf{x} = \int_{\partial\Omega} \frac{\partial v}{\partial \mathbf{n}} N_f \, d\sigma - \int_{\partial\Omega} v \frac{\partial N_f}{\partial \mathbf{n}} \, d\sigma = \int_{\partial\Omega} N_f \frac{\partial u}{\partial \mathbf{n}} \, d\sigma - \int_\Sigma h \frac{\partial N_f}{\partial \mathbf{n}} \, d\sigma$$

Inserting this equation into (4.21) gives

$$J(\Omega) = \int_\Omega g^2 + N_f f d\mathbf{x} + \int_\Sigma \frac{\partial v}{\partial \mathbf{n}} h d\sigma + \int_{\partial\Omega} N_f \frac{\partial u}{\partial \mathbf{n}} \, d\sigma. \tag{4.22}$$

Hence, in order to compute the cost functional and its gradient (2.7) we require only the normal derivative $\partial u / \partial \mathbf{n}$. Hence, its knowledge is sufficient to perform a first order optimization method. But the computation of the Hessian (2.8) requires also the second order derivatives $\partial^2 u / \partial \mathbf{n}^2$ and $\partial^2 u / (\partial \mathbf{n} \partial \mathbf{t})$.

The ansatz (4.19) leads to the normal derivative $\partial u / \partial \mathbf{n}$ according to

$$\frac{\partial u}{\partial \mathbf{n}} = \frac{\partial v}{\partial \mathbf{n}} + \frac{\partial N_f}{\partial \mathbf{n}}$$

with the Newton potential N_f defined via (4.18) and v satisfying the boundary value problem (4.20). We introduce the *single layer operator* $\mathcal{V}$ and the *double layer operator* $\mathcal{K}$ defined by

$$\begin{aligned} (\mathcal{V}u)(\mathbf{x}) &:= -\frac{1}{2\pi} \int_{\partial\Omega} \log \|\mathbf{x} - \mathbf{y}\| u(\mathbf{y}) d\sigma_{\mathbf{y}}, \\ (\mathcal{K}u)(\mathbf{x}) &:= \frac{1}{2\pi} \int_{\partial\Omega} \frac{\langle \mathbf{n}_{\mathbf{y}}, \mathbf{x} - \mathbf{y} \rangle}{\|\mathbf{x} - \mathbf{y}\|^2} u(\mathbf{y}) d\sigma_{\mathbf{y}}. \end{aligned}$$

Then, the normal derivative of v is given by the Dirichlet-to-Neumann map

$$\mathcal{V}\frac{\partial v}{\partial \mathbf{n}} = \Big(\frac{1}{2} + \mathcal{K}\Big)(h\chi_\Sigma - N_f), \tag{4.23}$$

where χ_Σ denotes the characteristic function with respect to the boundary Σ.

If we denote the function space of all squared integrable functions on $\partial\Omega$ with respect to the canonical inner product by $L^2(\partial\Omega)$ and the associated Sobolev spaces by $H^s(\partial\Omega)$, $s \in \mathbb{R}$, then, in this context, $\mathcal{V} : H^{-1/2}(\partial\Omega) \to H^{1/2}(\partial\Omega)$ defines an operator of the order -1 while $\frac{1}{2} + \mathcal{K} : H^{1/2}(\partial\Omega) \to H^{1/2}(\partial\Omega)$ defines an operator of the order 0.

Next, according to [19], due to zero Dirichlet boundary condition on Γ, we find the equation

$$\frac{\partial^2 u}{\partial \mathbf{n}^2} = -\kappa\left(\frac{\partial N_f}{\partial \mathbf{n}} + \frac{\partial v}{\partial \mathbf{n}}\right) - f \qquad \text{on } \Gamma,$$

that is $\partial^2 u/\partial \mathbf{n}^2$ can be derived directly from the first order derivative $\partial v/\partial \mathbf{n}$. Finally, from (4.19) we deduce

$$\frac{\partial^2 u}{\partial \mathbf{n}\partial \mathbf{t}} = \frac{\partial^2 v}{\partial \mathbf{n}\partial \mathbf{t}} + \frac{\partial^2 N_f}{\partial \mathbf{n}\partial \mathbf{t}}$$

with the unknown function $\partial^2 v/(\partial \mathbf{n}\partial \mathbf{t})$. It is recommendable to choose again a boundary integral formulation since we do not loose the regularity of $\partial v/\partial \mathbf{n}$. In accordance with [19, 36, 37], let the operators

$$\Big[\mathcal{V}, \tfrac{\partial}{\partial \mathbf{t}}\Big] : H^{-1/2}(\partial\Omega) \to H^{1/2}(\partial\Omega),$$
$$\Big[\tfrac{1}{2} + \mathcal{K}, \tfrac{\partial}{\partial \mathbf{t}}\Big] : H^{1/2}(\partial\Omega) \to H^{1/2}(\partial\Omega).$$

denote the commutators of $\mathcal{V}$ and $\frac{1}{2} + \mathcal{K}$. Then, differentiation of (4.23) with respect to the tangent vector gives the boundary integral equation

$$\mathcal{V}\frac{\partial^2 v}{\partial \mathbf{n}\partial \mathbf{t}} = \Big(\frac{1}{2} + \mathcal{K}\Big)\frac{\partial(h\chi_\Sigma - N_f)}{\partial \mathbf{t}} + \Big[\frac{1}{2} + \mathcal{K}, \frac{\partial}{\partial \mathbf{t}}\Big](h\chi_\Sigma - N_f) - \Big[\mathcal{V}, \frac{\partial}{\partial \mathbf{t}}\Big]\frac{\partial v}{\partial \mathbf{n}}. \tag{4.24}$$

5. Discretization

5.1. **Finite Dimensional Representation of Boundaries.** Since the infinite dimensional optimization problem cannot be solved directly, we replace it by a finite dimensional problem. Based on the polar coordinate approach, we can express the smooth function $r \in C^{2,\alpha}_{\text{per}}([0, 2\pi])$ by the Fourier series $r(\phi) = a_0 + \sum_{n=1}^{\infty} a_n \cos n\phi + a_{-n} \sin n\phi$. Hence, it is reasonable to take the truncated Fourier series

$$r_N(\phi) = a_0 + \sum_{n=1}^{N} a_n \cos n\phi + a_{-n} \sin n\phi. \tag{5.25}$$

as approximation of r. We mention that also other boundary representations like B-splines can be considered as well. The advantages of our approach is an exponential convergence $r_N \to r$ if the shape is analytical i.e., $\|r - r_N\|_{L^\infty([0,2\pi])} \lesssim q^N$ for an appropriate $q < 1$.

Since r_N has the $2N+1$ degrees of freedom $a_{-N}, a_{1-N}, \ldots, a_N$, we arrive at a finite dimensional optimization problem in the open set

$$A_N := \{a_{-N}, a_{1-N}, \ldots, a_N \in \mathbb{R} : r_N(\phi) > 0,\ \phi \in [0, 2\pi]\} \subset \mathbb{R}^{2N+1}.$$

Then, via the identification $r_N \Leftrightarrow \Omega_N$, the finite dimensional approximation of problem (1.4) reads as $J(\Omega_N) \to \min$. The associated gradients $\nabla J(\Omega_N)$ and Hessians $\nabla^2 J(\Omega_N)$ have to be computed with respect to all directions $dr, dr_1, dr_2 = \cos N\phi, \cos(N-1)\phi, \ldots, \sin(N-1)\phi, \sin N\phi$.

We shall employ a Newton scheme to solve the nonlinear equation $\nabla J(\Omega_N) = \mathbf{0}$, that is, the iteration is based on the following update rule

$$\Omega_N^{(n+1)} = \Omega_N^{(n)} - h^{(n+1)} \big(\nabla^2 J(\Omega_N^{(n)})\big)^{-1} \nabla J(\Omega_N^{(n)}). \tag{5.26}$$

Herein, the update has to be understood in terms of Fourier coefficients. Note that the step width $h^{(n+1)}$ is computed by a quadratic line search based on the information $J(\Omega_N^{(n+1)})$, $J(\Omega_N^{(n)})$ and $\nabla J(\Omega_N^{(n)})$.

5.2. **The Newton Potential.** The Newton potential N_f is supposed to be explicitly known or computed with sufficiently high accuracy. Since we require this potential as well as its gradient and Hessian, we cannot compute it just by globally continuous finite elements. But since we can choose the computational domain $\widehat{\Omega}$ fairly simple, one can use, for example, finite elements based on tensor products of higher order B-splines (in $[-R, R]^2$) or dual reciprocity methods.

5.3. **The Wavelet Galerkin Scheme.** Boundary element methods provide a common tool for the solution of boundary integral equations. In general, cardinal B-splines are used as ansatz functions in the Galerkin formulation. But discretizing the boundary integral equations (4.23) and (4.24) with respect to such *single-scale bases* yields densely populated system matrices. In combination with the ill-posedness of the single layer operator and its commutator, this implies at least a quadratic complexity for their solution. The crucial idea of the wavelet Galerkin scheme is a change of bases, i.e., applying appropriate (biorthogonal) wavelet bases instead of the traditional single-scale bases. Then, the arising system matrices become quasi-sparse and can be compressed without loss of accuracy, cf. [26, 27, 35].

For a fixed domain, we have to solve the boundary integral equations (4.23) and (4.24) several times, namely,

- the Dirichlet-to-Neumann map (4.23) applies to the state function and the associated $2N+1$ local shape derivatives, while
- (4.24) has to be evaluated one time for the state function.

Hence, an efficient realization discretizes both, the boundary integral operators on the left *and* right hand side of the given boundary integral equations. This requires a mixed formulation in order to achieve the optimal order of convergence. For the sake of simplicity we consider in the present paper only the case of piecewise constant and linear functions.

Exploiting polar coordinates, we introduce a parametrical representation of the boundary Γ in accordance with

$$\boldsymbol{\gamma} : [0,1] \to \Gamma, \quad s \mapsto \boldsymbol{\gamma}(s) := r(2\pi s) \left[\begin{smallmatrix} \cos(2\pi s) \\ \sin(2\pi s) \end{smallmatrix} \right].$$

The boundary Σ is parametrized likewise via a function $\boldsymbol{\sigma} : [0,1] \to \Sigma$.

For sake of simplicity in representation, we restrict ourselves now to the boundary Γ. The discretization with respect to the boundary Σ is treated analogously. We subdivide the boundary Γ into 2^l panels $\pi_{l,k} := \boldsymbol{\gamma}\big(2^{-l}[k,k+1)\big)$, where $k \in \triangle_l := \{0,1,\ldots,2^l-1\}$. We denote the space of the piecewise constants and linears defined on the given partition by $V_l^{(1)} = \operatorname{span} \Phi_l^{(1)}$ and $V_l^{(2)} = \operatorname{span} \Phi_l^{(2)}$. Herein, a single function of the collection $\Phi_l^{(d)} := \{\phi_{l,k}^{(d)} : k \in \triangle_l\}$ is given via $\phi_{l,k}^{(1)} = 2^{l/2} \chi_{\pi_{l,k}}$ and

$$\phi_{l,k}^{(2)}(\mathbf{x}) = 2^{3l/2} \begin{cases} s - 2^{-l}(k-1), & \mathbf{x} = \boldsymbol{\gamma}_i(s) \in \pi_{l,k-1}, \\ 2^{-l}(k+1) - s, & \mathbf{x} = \boldsymbol{\gamma}_i(s) \in \pi_{l,k}, \\ 0, & \text{elsewhere}, \end{cases}$$

respectively (see also Figure 5.2). Note that we use a L^2-normalization, i.e., $\|\phi_{l,k}^{(d)}\|_{L^2(\Gamma)} \sim 1$ for $d = 1, 2$.

By this construction we obtain two sequences of nested spaces $V_{l_0}^{(d)} \subset V_{l_0+1}^{(d)} \subset \ldots \subset L^2(\partial\Gamma)$, generating multiscale analyses, cf. [6]. We introduce suitable wavelet bases $\Psi_l^{(d)} := \{\psi_{l,k}^{(d)} : k \in \triangle_l\}$ which span complementary spaces $W_l^{(d)} := \operatorname{span} \Psi_l^{(d)}$ satisfying $V_l^{(d)} \oplus W_l^{(d)} = V_{l+1}^{(d)}$. For the matrix compression, these wavelet bases are required to provide *vanishing moments* in terms of

$$\int_\Gamma \big(\boldsymbol{\gamma}^{-1}(\mathbf{x})\big)^\alpha \psi_{l,k}^{(d)}(\mathbf{x}) d\sigma = 0, \quad 0 \le \alpha < \widetilde{d}.$$

According to [26], it suffices to consider piecewise constant wavelets with $\widetilde{d} = 3$ vanishing moments and piecewise linear wavelets with $\widetilde{d} = 2$ vanishing moments. Such wavelets have been constructed in [6]. They can be characterized by their refinement relation $\psi_{l,k}^{(d)} = \sum_j a_j \phi_{l+1,2k+j}^{(d)}$ via the *mask coefficients*

$$\begin{aligned} (a_{-2}, a_{-1}, \ldots, a_3) &= (-1/8, -1/8, 1, -1, 1/8, 1/8), \qquad d = 1, \\ (a_{-1}, a_0, \ldots, a_3) &= (-1/8, -1/4, 3/4, -1/4, -1/8), \quad d = 2, \end{aligned}$$

cf. Figure 5.2. It is well known [6] that the collections $\Psi_L^{(d)} := \bigcup_{l=l_0-1}^{L-1} \Psi_l^{(d)}$, where $\Psi_{l_0-1}^{(d)} := \Phi_{l_0}^{(d)}$, form uniformly stable bases in $L^2(\partial\Gamma)$. In fact, this *Riesz property* implies the existence of a corresponding *dual* multiresolution analysis. We refer to [6, 27, 35] for details.

We make the ansatz $\partial v/\partial \mathbf{n} = \Psi_L^{(1)} \mathbf{v}_L$ and $\partial^2 v/(\partial \mathbf{n} \partial \mathbf{t}) = \Psi_L^{(1)} \widetilde{\mathbf{v}}_L$. Then, introducing the system matrices

$$\begin{aligned} \mathbf{V}_L &:= (\mathcal{V}\Psi_L^{(1)}, \Psi_L^{(1)})_{L^2(\partial\Omega)}, & \mathbf{K}_L &:= \big((\tfrac{1}{2} + \mathcal{K})\Psi_L^{(2)}, \Psi_L^{(1)}\big)_{L^2(\partial\Omega)}, \\ \widetilde{\mathbf{V}}_L &:= \big(\big[\mathcal{V}, \tfrac{\partial}{\partial \mathbf{t}}\big]\Psi_L^{(1)}, \Psi_L^{(1)}\big)_{L^2(\partial\Omega)}, & \widetilde{\mathbf{K}}_L &:= \big(\big[\tfrac{1}{2} + \mathcal{K}, \tfrac{\partial}{\partial \mathbf{t}}\big]\Psi_L^{(2)}, \Psi_L^{(1)}\big)_{L^2(\partial\Omega)}, \end{aligned} \tag{5.27}$$

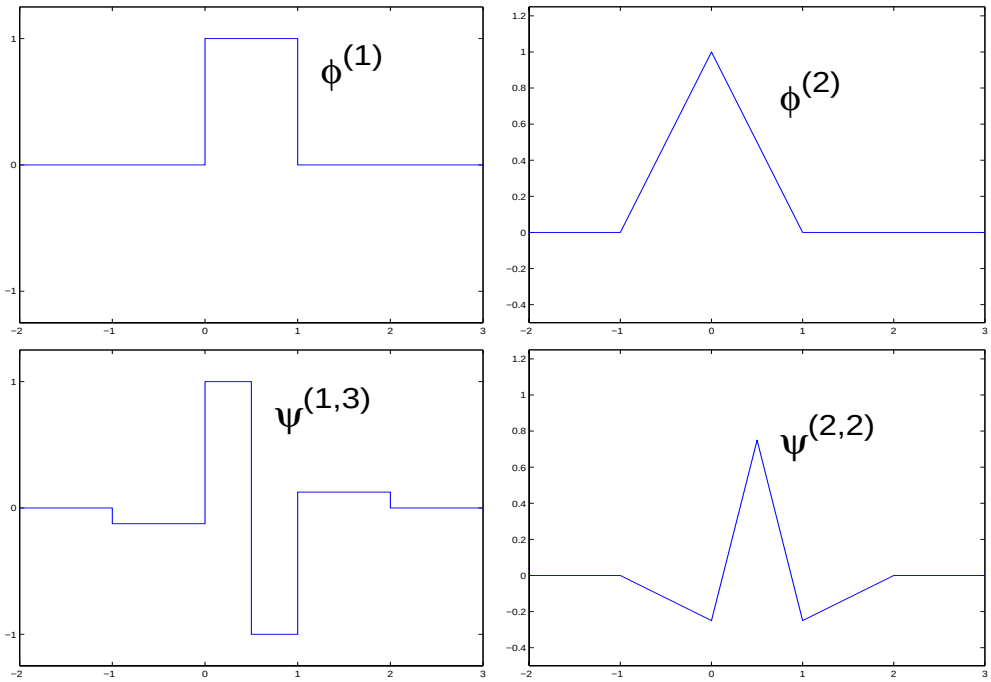

FIGURE 5.2. Piecewise constant and linear scaling functions respective wavelets.

the data vectors $\mathbf{u}_L := (g - N_f, \Psi_L^{(2)})_{L^2(\partial\Omega)}$, $\widetilde{\mathbf{u}}_L := (\partial(g - N_f)/\partial\mathbf{t}, \Psi_L^{(2)})_{L^2(\partial\Omega)}$, and the mass matrix $\mathbf{G}_L := (\Psi_L^{(2)}, \Psi_L^{(2)})_{L^2(\partial\Omega)}$, the boundary integral equation (4.23) corresponds to

$$\mathbf{V}_L \mathbf{v}_L = \mathbf{K}_L \mathbf{G}_L^{-1} \mathbf{u}_L,$$

while (4.24) corresponds to

$$\mathbf{V}_L \widetilde{\mathbf{v}}_L = \mathbf{K}_L \mathbf{G}_L^{-1} \widetilde{\mathbf{u}}_L + \widetilde{\mathbf{K}}_L \mathbf{G}_L^{-1} \mathbf{u}_L + \widetilde{\mathbf{V}}_L \mathbf{v}_L.$$

Consequently, we have to compute only four system matrices for each new domain, but solving the discrete systems several times with different data vectors. We mention that $\mathbf{G}_L^{-1}\mathbf{u}_L\Psi_L^{(d)}$ and $\mathbf{G}_L^{-1}\widetilde{\mathbf{u}}_L\Psi_L^{(d)}$ denote the L^2-othogonal projections onto $V_L^{(2)}$ of the given data $g - N_f$ and $\partial(g - N_f)/\partial\mathbf{t}$, respectively.

As mentioned above, the system matrices (5.27) are quasi-sparse. They can be compressed without loss of accuracy to $\mathcal{O}(2^L)$ nonvanishing matrix entries, see [26, 27, 35] for details. Actually, in accordance with [25, 27, 35], the over-all complexity of compressing and assembling the system matrices is still asymptotically linear. Moreover, based on the well known norm equivalences of wavelet bases, $\mathrm{diag}(\mathbf{V}_L^{\psi})$ and $\mathrm{diag}(\widetilde{\mathbf{V}}_L^{\psi})$ provide simple (diagonal) preconditioner for the given boundary integral equations [10, 12, 35]. We like to stress that, besides the difficulties of the net generation and the computation of second order derivatives, modern finite element method have the complexity $\mathcal{O}(2^{2L})$.

Theorem 5.1. *Let the domain Ω be fixed and sufficiently smooth. Then, the computational expense for solving* (4.23) *and* (4.24) *by the wavelet Galerkin scheme stays proportional to the number of unknowns.*

Assuming further the directions dr, dr_1, dr_2 sufficiently smooth and fixed, the discretization errors are given by

$$|(J - \overline{J})(\Omega)| \lesssim h_L^3,$$
$$|(\nabla J - \overline{\nabla J})(\Omega)[dr]| \lesssim h_L^2,$$
$$|(\Delta J - \overline{\Delta J})(\Omega)[dr_1, dr_2]| \lesssim h_L^2$$

provided that the numerically computed Newton potential $\overline{N_f}$ satisfies the pointwise estimates

$$\|N_f - \overline{N_f}\|_{L^\infty(\widehat{\Omega})} \lesssim h_L^3,$$
$$\|\nabla N_f - \overline{\nabla N_f}\|_{L^\infty(\widehat{\Omega})} \lesssim h_L^2,$$
$$\|\nabla^2 N_f - \overline{\nabla^2 N_f}\|_{L^\infty(\widehat{\Omega})} \lesssim h_L^2.$$

Herein, $h_L = 2^{-L}$ denotes the step width on the level L and $\overline{J}, \overline{\nabla J}, \overline{\Delta J}$ indicate the approximate solutions of the cost functional, its gradient and its Hessian.

Proof. The first statement is a consequence of [11, 26, 27]. The second statement has been proven in [19]. □ □

Remark 5.2. *We mention that the proof of the order of convergence with respect to the shape Hessian makes essential use of the fact that the Neumann data of the local shape derivatives are computed with the same accuracy than all other data. Since we plug only a piecewise constant approximation of the Neumann data of the state function into the Dirichlet-to-Neumann map* (4.23)*, it seems at first glance that one order is lost. However, exploiting a superconvergence result of* [9] *shows that this is not the case, see also* [19] *for more details. Nevertheless, this result is valid only with respect to two space dimensions. Therefore, in case of $n = 3$, we would realize in fact only an order of convergence $\mathcal{O}(h_L)$. Consequently, it is sufficient to use differentiation in order to compute $\partial^2 u/(\partial \mathbf{n} \partial \mathbf{t})$ from the Neumann data $\partial u/\partial \mathbf{n}$, which would require globally continuous ansatz functions also for the discretization of the Neumann data. Using (globally continuous) piecewise linear or bilinear ansatz functions for both, the Dirichlet and Neumann data, leads to the orders of convergence $\mathcal{O}(h_L^4)$ for the shape functional and its gradient and $\mathcal{O}(h_L^3)$ for the Hessian, provided that $\mathcal{K}$ is smoothing one order. But this is the case for the considered class of domains.*

6. Numerical Results

In our first example we consider the following free boundary value problem $\Delta u = 0$ in Ω, $u = 1$ on Σ, and $u = 0$, $\|\nabla u\| = const.$ on Γ. It indicates Bernoulli's exterior free boundary problem and models for example the growth of anodes in electrochemical processes. The interior boundary Σ is given by the parametric representation

$$\boldsymbol{\sigma} : [0,1] \to \Sigma, \qquad s \mapsto \boldsymbol{\sigma}(s) = \begin{bmatrix} 0.45\cos(2\pi s) \\ 0.3\sin(2\pi s)(1.25+\cos(2\pi s)) \end{bmatrix}.$$

This boundary is indicated by the dashed line in Figure 6. We compute the solution with respect to *const.* equal to all natural numbers in the interval $[1, 10]$. We like to stress that in this case ($f = 0$ and $g = const$), the shape functional itself can be computed only on the boundary $\partial\Omega$ since

$$\int_\Omega g^2 d\mathbf{x} = \frac{1}{2} g^2 \int_{\partial\Omega} \langle \mathbf{x}, \mathbf{n} \rangle d\sigma.$$

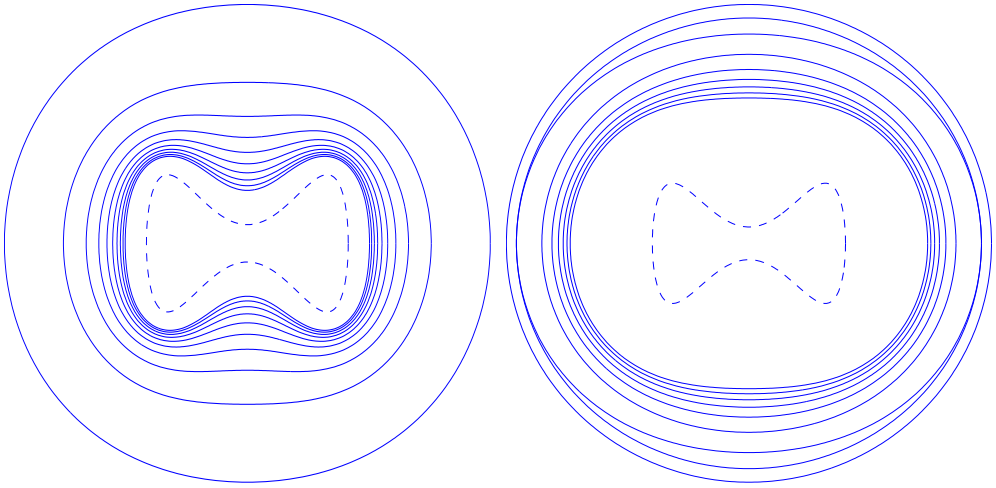

FIGURE 6.3. Computed free boundaries for Example 1 (left) and Example 2 (right).

The numerical setting is as follows. We discretize the free boundary via 65 Fourier coefficients ($N = 32$) and employ 1024 ($L = 10$) boundary elements on each boundary. We use the circle with radius 0.6 as initial guess of the Newton scheme. The Newton scheme is stopped if the norm of the actual gradient, measured with respect to $H^{1/2}(\Gamma)$, is less than 10^{-5}. We mention that this accuracy corresponds to a reduction of a factor 10^{-7} relative to the initial guess. The number of iterations and the computing times are tabulated in Table 6.1. Note that we do not need a line search for the considered values of *const.*, i.e., the step width $h^{(n)}$ in (5.26) is chosen always equal to 1. The resulting free boundaries are depicted in the left plot of Figure 6.3, where the outer boundary corresponds to *const.* $= 1$ and the inner one to *const.* $= 10$.

We also computed the minimum $\min_{\mathbf{x} \in \Gamma_N^\star} \kappa(\mathbf{x})$, which indicates a stable minimizer if it is positive. However, since the resulting boundary becomes more nonconvex if *const.* grows, this minimum decreases and becomes negative. However, if we compute the eigenvalues of the discrete Hessian, using $H^{1/2}(\Gamma)$-normalized Fourier series, we see that the minimal eigenvalue $\lambda_{\min}$ even increases when *const.* grows. This fact strongly indicates that the computed free boundaries are stable minimizers. Additionally we tabulated in Table 6.1 also the maximal eigenvalue $\lambda_{\max}$.

In the second example we choose $-\Delta u = const.$ in Ω, $u = 1$ on Σ, and $u = 0$, $\|\nabla u\| = 2$ on Γ. A suitable Newton potential is given by $N_f = -const.(x^2 + y^2)/4$. Likewise to the first example, we play with the inhomogenity *const.* as tabulated in Table 6.2. Moreover,

const.	$\min\kappa$	$\lambda_{\min}$	$\lambda_{\max}$	iterations	cpu-time
1	0.69	6.6	25	9	92 secs.
2	0.30	24	$1.2 \cdot 10^2$	7	73 secs.
3	-0.47	49	$3.2 \cdot 10^2$	7	79 secs.
4	-1.40	75	$6.4 \cdot 10^2$	6	70 secs.
5	-2.34	98	$1.1 \cdot 10^3$	7	89 secs.
6	-3.19	$1.2 \cdot 10^2$	$1.7 \cdot 10^3$	6	80 secs.
7	-3.90	$1.3 \cdot 10^2$	$2.5 \cdot 10^3$	8	100 secs.
8	-4.59	$1.4 \cdot 10^2$	$3.5 \cdot 10^3$	7	92 secs.
9	-5.21	$1.4 \cdot 10^2$	$4.7 \cdot 10^3$	7	90 secs.
10	-5.52	$1.5 \cdot 10^2$	$6.1 \cdot 10^3$	8	102 secs.

TABLE 6.1. Numerical results for Example 1.

const.	$\min\kappa - const./2$	$\lambda_{\min}$	$\lambda_{\max}$	iterations	cpu-time
0	0.30	24	125	7	73 secs.
0.5	0.28	24	113	7	77 secs.
1.0	0.25	24	102	7	78 secs.
1.5	0.22	24	89	7	76 secs.
2.0	0.18	24	75	8	91 secs.
2.5	0.14	23	59	9	97 secs.
3.0	$8.5 \cdot 10^{-2}$	20	40	8	86 secs.
3.46	$6.0 \cdot 10^{-6}$	7	24	9	97 secs.
3.48	$-2.0 \cdot 10^{-2}$	0.13	24	12	151 secs.

TABLE 6.2. Numerical results for Example 2.

we use the same setup as above. Note that also in the present case the shape functional can be computed by a boundary integral. Observing $\Omega = T \setminus S$ we conclude

$$\begin{aligned}\int_\Omega f N_f d\mathbf{x} &= const. \int_S \frac{x^2+y^2}{4} d\mathbf{x} - const. \int_T \frac{x^2+y^2}{4} d\mathbf{x} \\ &= C(S) - const. \int_0^{2\pi} \int_0^{r(\phi)} \frac{\rho^3}{4} d\rho\, d\phi \\ &= C(S) - \frac{const.}{16} \int_0^{2\pi} r(\phi)^4 d\phi.\end{aligned}$$

Since $C(S)$ is constant for all admissible domains Ω we may discard its evaluation.

The number of iterations and the computing times are tabulated in Table 6.2. Likewise to above the line search becomes never active. The resulting free boundaries are depicted in the right plot of Figure 6.3, where the diameter of the free boundaries increases if constant *const.* increases. One figures out of Table 6.2 that the minimum $\min_{\mathbf{x}\in\Gamma_N^*} \kappa(\mathbf{x}) - const./2$ decreases if *const.* increases. This minimum is about zero if $const. = 3.46$. The largest value for which the Newton scheme converges is $const. = 3.48$. We see that in this case

the minimal eigenvalue of the discrete Hessian is nearly zero. All solutions except the last one are stable minimizers according to Corollary 3.5.

7. Conclusion

In the present paper we proposed a Newton scheme for the efficient solution of free stationary boundary problems. Numerical results show that we realized in fact a fast and robust solver for the considered class of problems. Additionally, we provided new results concerning the stability of the minimizers.

References

[1] H.W. Alt and L.A. Caffarelli. Existence and regularity for a minimum problem with free boundary. *J. reine angew. Math.*, 325:105–144, 1981.

[2] N.V. Banichuk and B.L. Karihaloo (1976). Minimum-weight design of multi-purpose cylindrical bars. *International Journal of solids and Structures*, 12:267–273.

[3] M. Brühl. Explicit characterization of inclusions in electrical impedance tomography. *SIAM J. Math. Anal.*, 32:1327–1341, 2001.

[4] M. Brühl and M. Hanke. Numerical implementation of two noniterative methods for locating inclusions by impedance tomography. *Inverse Problems*, 16:1029–1042, 2000.

[5] R. Chapko and R. Kress. A hybrid method for inverse boundary value problems in potential theory. Preprint Uni Göttingen, to appear,

[6] A. Cohen, I. Daubechies, and J.-C. Feauveau. Biorthogonal bases of compactly supported wavelets. *Pure Appl. Math.*, 45:485–560, 1992.

[7] O. Colaud and A. Henrot. Numerical approximation of a free boundary problem arising in electromagnetic shaping. *SIAM J. Numer. Anal.*. 31: 1109–1127, 1994.

[8] D. Colton and R. Kress. Integral equation methods in scattering theory. Published in: Pure and Applied Mathematics Chichester, Wiley, 1983.

[9] M. Crouzeix and F.-J. Sayas. Asymptotic expansions of the error of spline Galerkin boundary element methods. *Numer. Math.*, 78:523–547, 1998.

[10] W. Dahmen. Wavelet and multiscale methods for operator equations. *Acta Numerica*, 6:55–228, 1997.

[11] W. Dahmen, H. Harbrecht and R. Schneider. Compression techniques for boundary integral equations – optimal complexity estimates. *Preprint SFB 393/02-06, TU Chemnitz*, 2002. submitted to SIAM J. Numer. Anal.

[12] W. Dahmen and A. Kunoth. Multilevel preconditioning. *Numer. Math.*, 63:315–344, 1992.

[13] M. Dambrine. On variations of the shape Hessian and sufficient conditions for the stability of critical shapes. *RACSAM, Rev. R. Acad. Cien. Serie A. Mat.* 96, No.1, 95–121, 2002.

[14] M. Delfour and J.-P. Zolesio. *Shapes and Geometries.* SIAM, Philadelphia, 2001.

[15] K. Eppler. Boundary integral representations of second derivatives in shape optimization. *Discussiones Mathematicae (Differential Inclusion Control and Optimization)*, 20:63–78, 2000.

[16] K. Eppler. Optimal shape design for elliptic equations via BIE-methods. *J. of Applied Mathematics and Computer Science*, 10:487–516, 2000.

[17] K. Eppler (2000). Second derivatives and sufficient optimality conditions for shape functionals. *Control and Cybernetics.* 29:485–512.

[18] K. Eppler and H. Harbrecht. Numerical solution of elliptic shape optimization problems using wavelet-based BEM. *Optim. Methods Softw.*, 18:105-123, 2003.

[19] K. Eppler and H. Harbrecht. 2nd Order Shape Optimization using Wavelet BEM. *Preprint 06-2003, TU Berlin*, 2003. submitted to Optim. Methods Softw.

[20] K. Eppler and H. Harbrecht. Exterior Electromagnetic Shaping using Wavelet BEM. *Technical Report 13-2003*, Preprint Series of the Institute of Mathematics, TU Berlin, 2003. to appear in Math. Meth. Appl. Sci.

[21] K. Eppler and H. Harbrecht. Fast wavelet BEM for 3d electromagnetic shaping. *Bericht 03-9*, Berichtsreihe des Mathematischen Seminars der Christian-Albrechts-Universitt zu Kiel, 2003. to appear in Appl. Numer. Math.

[22] K. Eppler and H. Harbrecht. A regularized Newton method in electrical impedance tomography using shape Hessian information. *WIAS-Preprint No. 943*, WIAS Berlin, 2004. submitted to Control & Cybernetics.

[23] K. Eppler and H. Harbrecht. Shape optimization in 3D electrical impedance tomography. *WIAS-Preprint 963*, WIAS Berlin, 2004. submitted to Proceeding of IFIP TC 7.2 conference.

[24] M. Flucher and M. Rumpf. Bernoulli's free-boundary problem, qualitative theory and numerical approximation. *J. reine angew. Math.*, 486:165–204, 1997.

[25] H. Harbrecht. Wavelet Galerkin schemes for the boundary element method in three dimensions. *PHD Thesis, Technische Universität Chemnitz, Germany*, 2001.

[26] H. Harbrecht, F. Paiva, C. Pérez, and R. Schneider. Biorthogonal wavelet approximation for the coupling of FEM-BEM. *Numer. Math.*, 92:325–356, 2002.

[27] H. Harbrecht and R. Schneider. Wavelet Galerkin Schemes for 2D-BEM. In *Operator Theory: Advances and Applications*, volume 121. Birkhäuser, (2001).

[28] J. Haslinger, T. Kozubek, K. Kunisch and G. Peichl. Shape optimization and fictitious domain approach for solving free boundary value problems of bernoulli type. *Computational Optimization and Applications*, 26:231–251, 2003.

[29] F. Hettlich and W. Rundell The determination of a discontinuity in a conductivity from a single boundary measurement. *Inverse Problems.* 14:67–82, 1998.

[30] R. Kress. *Linear Integral Equations.* Springer-Verlag, Berlin-Heidelberg, 1989.

[31] V.G. Maz'ya and T.O. Shaposhnikova. *Theory of multipliers in spaces of differentiable functions.* Pitman, Boston, 1985.(Monographs and Studies in Mathematics, 23. Pitman Advanced Publishing Program. Boston - London - Melbourne: Pitman Publishing Inc. *XIII*, 344 p. (1985))

[32] A. Novruzi and J.R. Roche. Second derivatives, Newton method, application to shape optimization. INRIA-report No. 2555 (1995)

[33] M. Pierre and J.-R. Roche Computation of free surfaces in the electromagnetic shaping of liquid metals by optimization algorithms. *Eur. J. Mech, B/Fluids*, 10: 489–500, 1991.

[34] J.-R. Roche and J. Sokolowski Numerical methods for shape identification problems. *Control Cybern.* 25:867–894, 1996.

[35] R. Schneider. *Multiskalen- und Wavelet-Matrixkompression: Analysisbasierte Methoden zur Lösung großer vollbesetzter Gleichungssyteme.* B.G. Teubner, Stuttgart, 1998.

[36] H. Schulz, C. Schwab and W.L. Wendland. An extraction technique for boundary element methods. In W. Hackbusch and G. Wittum, editors, *Boundary Elements: Implementation and Analysis of Advanced Algorithms*, pages 219–231, 1996.

[37] C. Schwab and W.L. Wendland. On the extraction technique in boundary integral equations. *Math. Comp.*, 68:91–122, 1999.

[38] J. Sokolowski and J.-P. Zolesio. *Introduction to Shape Optimization.* Springer, Berlin, 1992.

[39] T. Tiihonen. Shape optimization and trial methods for free-boundary problems. *RAIRO Model. Math. Anal. Numér.*, 31(7):805–825, 1997.

[40] H. Triebel. *Theory of function spaces.* Birkhäuser, Basel-Boston-Stuttgart, 1983.

[41] J. Wloka. *Partial Differential Equations.* Cambridge University Press, Cambridge, 1987.